eTransportation 4 (2020) 100057

Contents lists available at ScienceDirect

eTransportation

journal homepage: www.journals.elsevier.com/etransportation

A scalable, causal, adaptive rule-based energy management for fuel cell hybrid railway vehicles learned from results of dynamic programming☆

Hujun Peng [a, *], Jianxiang Li [a], Andreas Thul [a], Kai Deng [a], Cem Ünlübayir [c], Lars Löwenstein [b], Kay Hameyer [a]

[a] Institute of Electrical Machines (IEM), RWTH Aachen University, Aachen, Germany
[b] Siemens Mobility GmbH, Vienna, Austria
[c] Chair for Electrochemical Energy Conversion and Storage Systems, Institute for Power Electronics and Electrical Drives (ISEA), RWTH Aachen University, Germany

ARTICLE INFO

Article history:
Received 10 February 2020
Received in revised form
24 March 2020
Accepted 14 April 2020
Available online 7 May 2020

Keywords:
Energy management
Fuel cell hybrid trains
Rule-based strategy
Dynamic programming
Scalability

ABSTRACT

A scalable, causal, adaptive rule-based energy management strategy for fuel cell hybrid trains is developed. The rules of this strategy are initiated by the results of two-dimensional dynamic programming under different driving conditions and utilize the convexity of the characteristic specific consumption curve of the fuel cell system. According to the strategy, the fuel cell power follows the estimated average load power. This average value is updated each time when the train leaves a station by using prior knowledge, which ensures its causality. Furthermore, the power demand due to the gradient slope is excluded while estimating the average value because the gravitational energy is recyclable. In this way, the fuel cell system works more stably without being influenced by the strongly changeable power demand due to the gradient slopes. In order to avoid over-charging of batteries during long hold time, which is often the case for regional railway vehicles, the pre-known driving, holding, and travel time available in railway transportation are used to improve the estimation of the average values. After comparison with the results of dynamic programming, an excellent fuel economy is observed under different driving cycles and weather. More consumption of 0.01% and 0.09% in summer and winter, respectively, compared to dynamic programming, results under a typical driving cycle of regional railway vehicles in Berlin. Because the rules are based on the component characteristics, this strategy can be transferred to other vehicle configurations or driving situations without a loss of effectiveness. In addition to the excellent fuel economy, the lifetime of fuel cell systems benefits from its less dynamic operation.

1. Introduction

1.1. Background and motivations

About 40% of the railway network in Germany is not electrified. More electrification of the railway network is proposed to reduce carbon dioxide emissions, [1]. Nevertheless, to fully electrify railway networks, especially for parts with low and medium traffic, is not economically beneficial. Therefore, it is a promising short-term alternative to replace combustion engine-driven vehicles with hydrogen-powered vehicles without high investment to completely electrify the entire network. So far, the Proton Exchange Membrane (PEM) fuel cell hybrid trains have been prototyped and commercialized worldwide. In June 2019, East Japan Railway Company declared that it is financing in developing a two-car trainset utilizing fuel-cell technology from Toyota, expecting to start tests by 2021 and have commercially-viable technology available by 2024 [2]. In September 2016, Alstom unveiled their newly produced iLint train, manufactured at the factory in Salzgitter. In September 2018, the operation of the

☆ This work is funded by the German Federal Ministry for Economic Affairs and Energy (BMWi) under the National Innovation Program Hydrogen and Fuel Cell Technology (NIP) with the funding numbers of 03B10502B and 03B10502B2. The authors gratefully acknowledge the support by Siemens AG and NIP.

* Corresponding author.
E-mail address: hujun.peng@iem.rwth-aachen.de (H. Peng).

https://doi.org/10.1016/j.etran.2020.100057
2590-1168/

trains was launched in Lower Saxony, Germany [3]. Siemens is working on Mireo to substitute combustion engine-driven trains, and a fuel cell variant with 200 kW rated fuel cell power is designed in partnership with Ballard. This hybrid train is supposed to begin its operation after 2021, which is the focus of this paper [4]. The fuel cell hybrid railway vehicles of Siemens is planned work under charge-sustaining conditions. In other words, the average load power is covered by the fuel cell systems, while the transient power demand during acceleration or regenerative braking operation is supported by the battery systems. Accordingly, the performance of the driveline can be improved by optimizing the distribution of load power between the battery systems and the fuel cell systems. In addition to hydrogen consumption minimization, it is beneficial to operate fuel cells less dynamically, to prolong the fuel cell lifetime [5].

1.2. Literature review

Two types of energy management strategies: optimization-based methods and rule-based methods are found in literature reviews [6,7]. In the rule-based methods, a series of heuristic rules are defined to determine the control, basing on human experience, boundary limitations, and safety concerns. Their advantage lies in robustness and low computational load, which enables them widely adopted in commercial hybrid vehicles like Prius [8] and Toyota Mirai [9]. Wang. et al. implement the rule-based strategies for fuel cell hybrid vehicles, with various mechanisms integrated [10]: considers the criteria of the remaining capacity, the demand power, and the power capability of the energy storage systems [11], adopts the Markov prediction method [12,13], use a finite state machine (FSM)-based energy management strategy. However, the parameters of the rules are based on heuristic experiences, and can not be transferred to other system configurations and driving conditions without loss of functionality. More crucial is that the fuel cell system is frequently switched on and off, which shortens the fuel cell lifetime and is in the praxis not reasonable. Furthermore, the parameters of the rule-based methods can be optimized by using the evolutionary algorithm to improve their performance. In Ref. [14], the parameters of membership functions of fuzzy logic rules are optimized. Nevertheless, the optimized parameters are related to the driving cycles for training, which restricts the adaptivity of the rule-based methods under changeable driving conditions. In order to avoid the affects of heuristic experience on the functionality of the rule-based strategies, the experience can be extracted from offline optimization-based results. In Ref. [15], dynamic programming is utilized to derive the rule-based energy management strategy for an electric city bus with a hybrid energy storage system, including a battery and a supercapacitor. However, the extracted rules are dependent on specific driving cycles, and then can not be scaled or transferred if the vehicle configuration or driving conditions change.

The optimization-based methods include both the global optimization-based methods and the local optimization-based methods. The global optimization methods can determine the global optimum solution by utilizing pre-known load information about the whole driving cycle. The most important ones are dynamic programming and Pontryagin's minimum principle (PMP)-based methods. Dynamic programming solves process optimization problems by utilizing Bellman's principles of optimality [16]. With interpolation used to estimate the cost-to-go function of new states, the algorithm is implemented parallelly to reduce computation time [17]. To fully satisfy the precondition of without after-effect before using dynamic programming, two-dimensional dynamic programming is designed to consider constraints on the change rate of fuel cell power [18]. However, because the solutions of dynamic programming are optimized for a pre-known driving cycle, they can be applied as a reference for real-time strategies. For the PMP-based methods, the control input is determined to minimize the Hamiltonian function at each time instant. However, the evaluation of the initial co-state strongly influences the solution quality if driving cycles are not priorly known.

For the local optimization-based methods, control is calculated by minimizing a predefined cost function, which is based on assumed equivalent factors of the battery energy consumption. Generally, for real-time applications, computational load and memory resources have to be considered to formulate the cost function suitably. The equivalent consumption minimization strategy (ECMS) is the most prominent one, which transforms battery power into an equivalent fuel consumption rate with the help of equivalent factors [19]. It is most challenging to estimate the equivalent factors because the evaluation of the equivalent factors greatly determines its performance. As found in the literature, the equivalent factors can be adjusted by using PI-controller based on the offline optimized state of charge (SoC) trajectory [20], corresponding to different driving conditions [21]. Besides ECMS, the adaptive PMP-based strategy belongs to the local optimization-based methods. It is described in Refs. [22] that ECMS is a simplified version of the PMP-based method. Similar to ECMS, the quality of estimation of the co-state influences the performance of the PMP-based method strongly. It is common to use PI-controllers to adjust the co-state [23]. However, the parameters of the PI-controller are not suitable for different driving conditions. Furthermore, these local optimization-based methods can be integrated into model predictive control (MPC) [24]. Thereby, the deviation of SoC from a reference value or an optimized SoC trajectory from prediction patterns is considered in the cost function. However, a fixed reference value restricts the optimality of strategies, as learned from offline results, and the optimized SoC trajectory relies on the quality of the prediction patterns. Besides, the requirement on real-time capability and limits by the available computational resources onboard restricts the horizontal length to be predicted in MPC.

Nowadays, the main research trend in the area of the energy management is to obtain optimal solutions in real-time applications [25]. Subsidiary adaption tools like intelligent traffic systems, pattern recognition, and prediction/estimation are combined with optimization-based methods to improve the performance of strategies [25]. However, on the one side, the effectiveness of these subsidiary tools relies on offline training efforts. Therefore, the transferability of the strategy to other driving conditions and different aging component states is not ensured. On the other side, the necessary communication infrastructure is not yet ready for big data communication.

Overall, the strategies adopted for commercial hybrid vehicles are restricted to the rule-based methods because of low computational burden and robustness, as for the Toyota Mirai [9], Prius [8], and Alstom Coradia iLint [26]. Compared with optimization-based methods, the inferiority of the rule-based methods have been expressed in Ref. [27,28]. The most important justifications for the conclusion are that the rules are extracted based on human experience, which restricts optimality and adaptivity of the rule-based methods. The fundamental reason for this prejudice is that the rules in the reviewed literature are assumed to be based on the engineer experience rather than analytically and quantitatively derived. Due to the lacking quantitative formulation, the scalability and adaptivity of the rule-based method are underestimated.

1.3. Main work

In order to overcome the shortcomings of rule-based methods, a quantitative formula based on the convexity of the specific consumption curve of fuel cell systems instead of human experience is

developed for the rule-based strategy. The rules are initiated by the results of dynamic programming, which is implemented for different driving cycles, weather, and rate limits of fuel cell systems. According to the strategy, the fuel cell power follows a corrected load power average value. Thereby, the available terrain information and pre-known information about driving, holding, and travel time, which are the case in railway transportation, are incorporated to correct the average estimates of load power. This incorporation helps to reduce the oscillation of working points of fuel cell systems, to prolong the fuel cell lifetime without loss of fuel efficiency. Moreover, two-dimensional dynamic programming is used as a reference to prove the effectiveness of the purposed strategies for different driving conditions, rate limits of fuel cell systems, and aging conditions. Simulation results show that this rule-based strategy can achieve an excellent fuel economy on the one side and maintains the fuel cell system to work with much less dynamic on the other side. More important is that this strategy can be scaled or transferred to different system configurations, driving conditions without loss of functionality. Moreover, this strategy is applied online.

1.4. Paper organization

The paper is organized as follows: In section 2, the driveline configuration related to energy management is briefly introduced. In section 3, the two-dimensional dynamic programming is used to determine the optimal strategy. Thereby, different driving cycles under different weather are used, and generic experience drawn from their results is given. In section 4, the rules learned from the results of dynamic programming are detailedly derived. Thereby, a quantitative analytical formula to estimate the average load power is step by step improved and mathematically justified. In section 5, the functionality of this rule-based strategy under different driving cycles, weather, rate limits of fuel cell systems, and aging conditions are approved by comparing simulation results to that of dynamic programming. Discussion based on the results will be given. In section 6, the conclusion and the possible outlook are given.

2. Driveline modeling

Fig. 1 displays the schematic of the driveline, which corresponds to a parallel hybrid structure. In order to analyze the effect of energy management on the fuel economy of hybrid trains, it is general to model the most components of the driveline stationary except SoC and the train velocity, with dynamic in other components not considered. Due to symmetry, a half train instead of the whole train is modeled in the following, as shown in Fig. 2. The modeling of components will be described in detail in the subsequent sections.

2.1. Environment model

In the environment model, driving cycles and slope profiles of three routes in Germany are defined, as presented in Fig. 3. The driving cycle 1 goes downhill and then uphill by trend, the driving cycle 2 goes uphill and then downhill, and the driving cycle 3

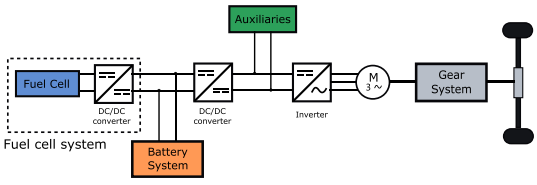

Fig. 1. System configuration of a hybrid train.

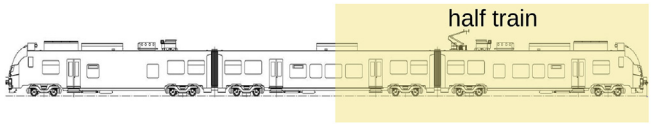

Fig. 2. A half train.

belongs to a regional railway vehicle in Berlin, which has a much smaller slope than the first two. These driving cycles were obtained by dynamic programming, with their route parameters, waiting times, and maximum acceleration considered, which is standard technology for velocity optimization. Other relevant environmental parameters include ambient temperature, number of passengers.

2.2. Longitudinal dynamic

The various forces acting on the vehicle are illustrated in Fig. 4. The forces acting on the train include several resistant forces and traction force F_x acting on wheels. The resisting forces on the train include rolling resistance F_r, uphill resistance F_g, aerodynamic drag F_{air}. During mechanical braking, there is also resistance force represented by F_b. The positive direction for the resistance forces is defined against the direction of travel. The longitudinal dynamics is described by (1):

$$F_a = F_x - F_r - F_{air} - F_g - F_b \tag{1}$$

$$m \cdot \frac{dv}{dt} = F_x - \mu_r mg\cos(\varphi) - 0.5 \cdot \rho_{air} C_d A_f v^2 - mg\sin(\varphi) - F_b$$

where F_a is the net force for acceleration, m the train mass, μ_r the rolling resistance coefficient, ρ_{air} the air density, C_d the aerodynamic coefficient, g the gravitational acceleration, A_f the front area, F_x the traction force on wheels, and φ the angle of slope, which is related to the slope as follows:

$$\varphi = \arctan(\text{slope}). \tag{2}$$

The above mentioned parameters can be found in Table 1.

2.3. Electrical machines

A half train is driven by three high-speed asynchronous machines, each with a peak power of 300 kW. The machines are modeled stationary because of the much shorter machine time constant when compared to the longitudinal dynamic. In total, four tables, as presented in Fig. 5, are used, which result from Finite Element Analysis. Besides the power loss in the machines, the other three lookup tables are necessary to determine the loss in inverters. The motor current influences the inverter loss directly, and the power factor influences the loss distribution between IGBT and diode. The motor voltage determines the modulation degree, which then influences the inverter loss. The gear system has a ratio of 10 with an assumed constant efficiency value of 0.98, and the vehicle wheel radius is 0.425 m. With the help of these parameters, the motor torque can be transformed to the traction force on the wheels. All the parameters related to the machines are summarized in Table 2.

2.4. DC/AC inverter

The inverter loss is dependent on various variables, including machine current, machine voltage, switching frequency or machine speed, power factor, semiconductor temperature, and DC-link

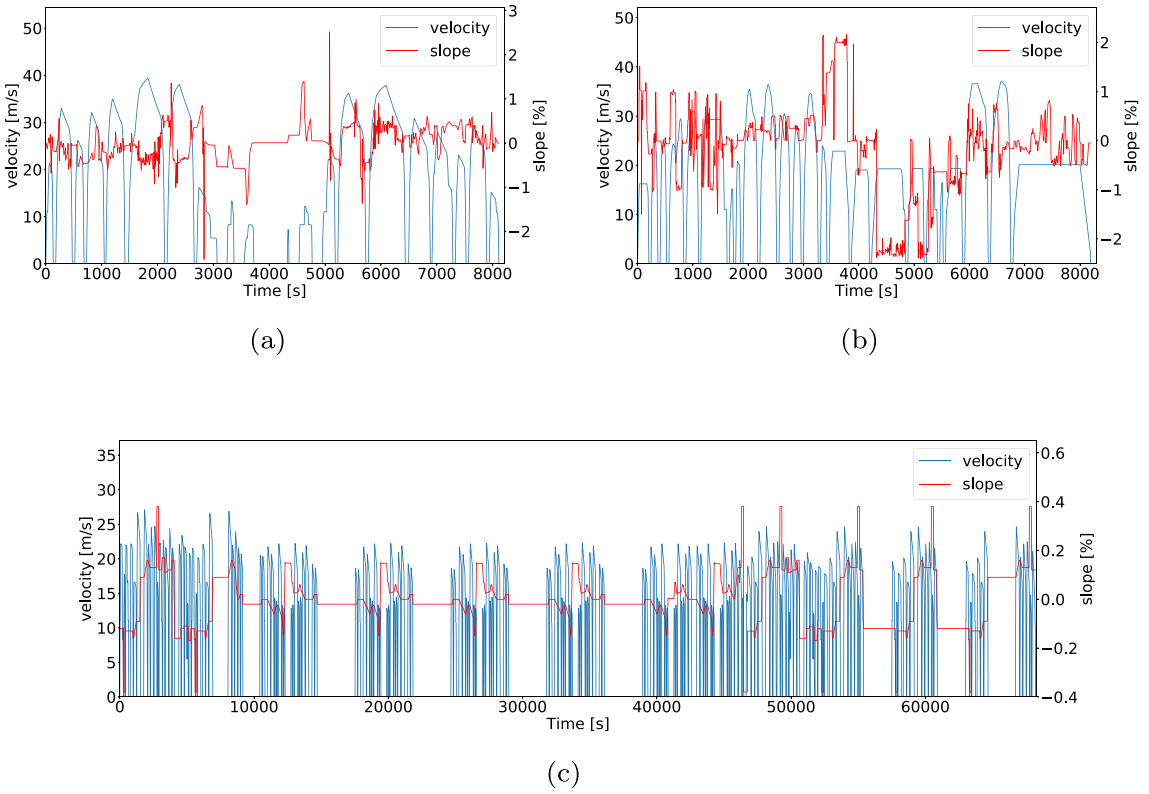

Fig. 3. Driving cycles: (a) driving cycle 1 with distance of 145.8 km and travel time of 8110 s, (b) driving cycle 2 with a distance of 154 km and travel time of 8192 s, (c) driving cycle 3 with a distance 584.5 km and travel time of 68213 s.

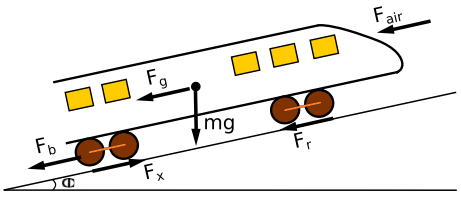

Fig. 4. Forces acting on the train.

Table 1
Parameters related to longitudinal dynamic.

parameters	symbols	values	units
train mass (with passengers included)	m	60000	kg
gravitational acceleration	g	9.81	m/s^2
rolling resistance coefficient	μ_r	0.0015	–
air density	ρ_{air}	1.4	kg/m^3
aerodynamic coefficient	C_d	0.15	–
front area	A_f	10	m^2

voltage. Nevertheless, temperature and DC-link voltage are in practice controlled to be constant. Therefore, four-dimensional lookup tables with the machine current, machine voltage, machine speed, power factor as inputs are utilized to model the inverter loss. The lookup tables result from a simulation with the help of software Plecs, and the simulated model is displayed in Fig. 6. Three alternate current sources are used as the load instead of motors, with a phase shift of 120° to each other. Through modulation control, the power factor and the amplitude of phase voltage can be changed. The influence of the power factor and motor speed on loss is also displayed, based on a working point with voltage and current equal to 350 V and 200 A. It is worth mentioning that the switching frequency is adjusted proportional to the motor speed, to keep the switching loss of the converter low at low motor speed. The switching frequency is 10 times the fundamental frequency of the current supply. The semiconductor has a breakdown voltage of 3300 V and a rated corrector current of 450 A, whose datasheet corresponds to the product of Infineon named FF450R33T3E3.

2.5. Auxiliary consumption

The auxiliary systems are used to implement the non-driving function of the train including creating a thermally comfortable environment. This includes compressors, heating, air conditioning, and ventilation systems. In order to calculate the energy consumption of an air conditioning system, consideration must be given to the thermal power introduced into the passenger compartment: heat conduction and convection, radiation, passenger heat tranfer, ventilation and the heat from electrical components [29]. In this work, since the focus lies on hybrid strategies, we used a static thermal model to simplify the calculation of energy consumption. We assume −5°C in winter, 35°C in summer, and 21°C in the cabin. Energy consumption can be estimated by calculating with heat flow and coefficient of power. In the simulation, we estimate that the power, including the onboard electrical consumers, is 83 kW in winter and 55 kW in summer.

2.6. DC/DC converter

For determining the DC/DC converter loss, the coupling between thermal and electrical modeling is taken into account. A thermal network is used to implement the thermal modeling and the heatsink temperature is set to be 40°C. In order to consider the

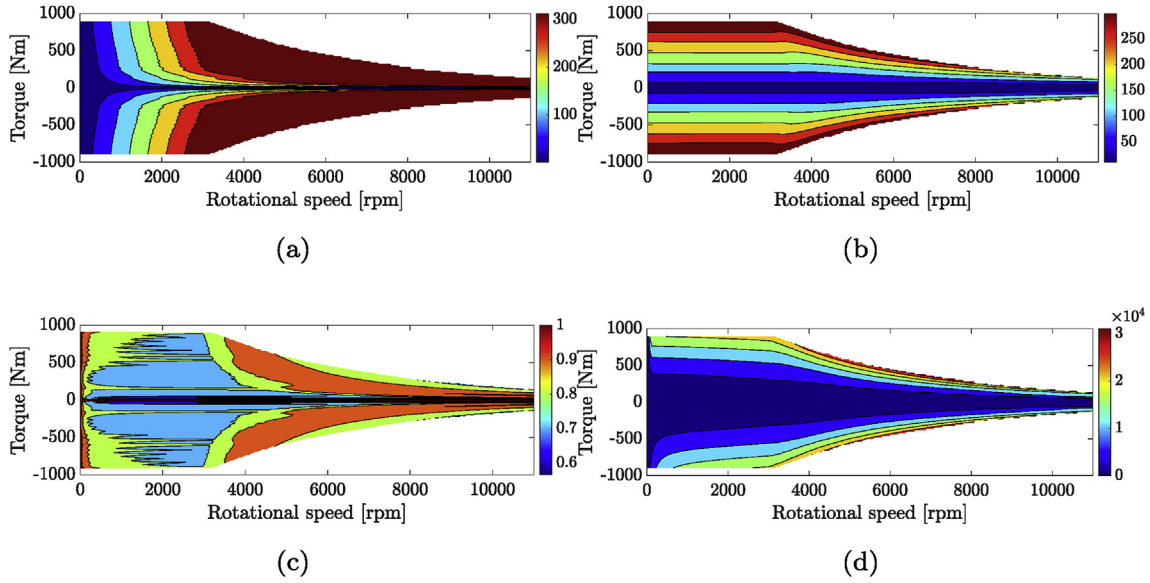

Fig. 5. Electrical machines characteristics: (a) Electrical machine voltage in V, (b) Electrical machine current in A, (c) Electrical machine power factor, (d) Electrical machine loss in W.

Table 2
Parameters related to electrical machines.

parameters	values	units
number of poles	4	–
rated power (kW)	220	kW
maximal power (kW)	300	kW
rated rotational speed	3200	rpm
maximal rotational speed	12000	rpm
gear ratio	10	–
gear efficiency	0.98	–
number of motors	3	–
wheel radius	0.425	m

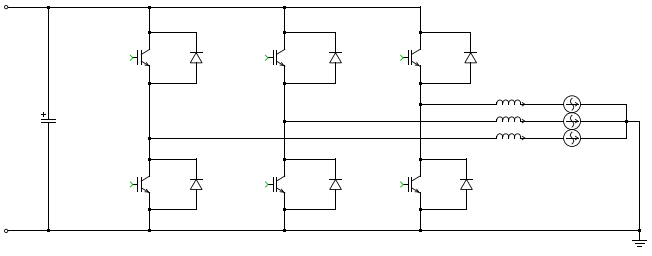

Fig. 6. Simulated model of DC/AC inverter in Plecs.

effect of the nonlinearity on the loss, lookup tables resulted from simulation, whose model is displayed in Fig. 8, are used. The semiconductor module is the same as used in the inverter. Parameters related to the loss are listed in Table 3.

Basically, the converter loss depends on the load current, battery voltage, DC-link voltage, and semiconductor temperature. The loss look-tables, with the battery voltage equal to its nominal value of 850 V, are presented in Fig. 7. The loss under different temperatures is shown, based on an operational point with the load current and DC-link voltage equal to 350 A and 1200 V.

2.7. Fuel cell system

The used PEM fuel cell system has a nominal power of 200 kW and an own DC/DC converter to control the output power. As the focus of this paper lies in the design of energy management strategy to improve fuel economy, instead of the effects of strategies on fuel cell aging, a static model of the fuel cell without an aging model is used within the simulation model. In other words, the electrochemistry mechanisms and complicated thermodynamic are not considered. The specific consumption curve shown in Fig. 9 is used to calculate the consumption. The convexity of the consumption curve can be drawn from Fig. 9b, which can be mathematically formulated as:

$$\dot{m}_{H_2}\left(\alpha \cdot P_{fc,1} + (1-\alpha)\cdot P_{fc,2}\right) < \alpha \cdot \dot{m}_{H_2}\left(P_{fc,1}\right) + (1-\alpha)\cdot \dot{m}_{H_2}\left(P_{fc,2}\right), \tag{3}$$

where $\dot{m}_{H_2}$ represents the mass flow depending on the net fuel cell power.

2.8. Battery system

The battery model of the lithium-ion high-performance cell used is parameterized with real measurement data. To obtain the parameters, electrochemical impedance spectroscopies and pulse tests were performed on single cells. Within the battery simulation model, an equivalent circuit model with 3 R−C branches is used, as shown in Fig. 10. Also it is assumed that during operation, compensation currents between battery cells connected in parallel are not taken into account. The cells are interconnected to modules, which are combined into a battery system with an total capacity of 200 kWh and a nominal voltage of 850 V. The open circuit voltage and various resistances of the whole battery system are displayed in Fig. 11. With the active liquid cooling, the temperature of the battery pack is controlled to be at 25°C, and thermal modeling is neglected.

3. Two-dimensional dynamic programming

Before introducing the adaptive rule-based strategy, two-dimensional dynamic programming is used to determine the optimal strategy. In most literature about energy management for

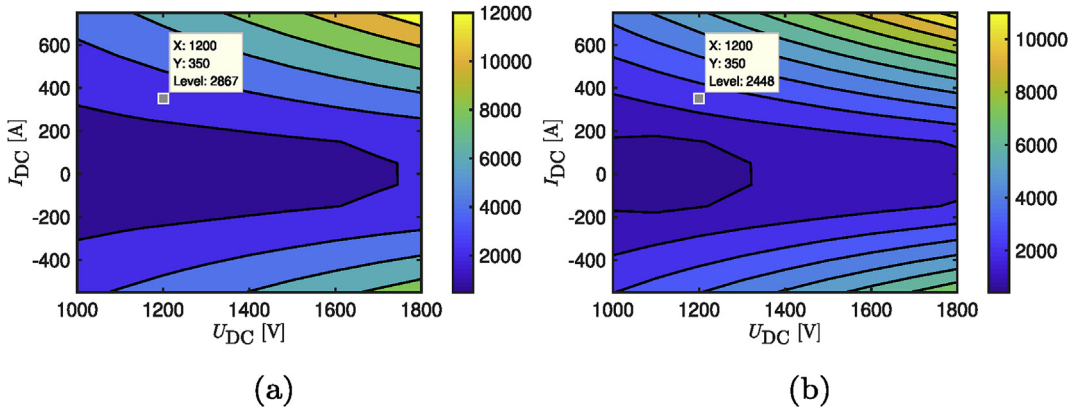

Fig. 7. DC/DC converter loss in W depending on voltage and load current at DC-link: (a) under 150°C, (b) under 80°C.

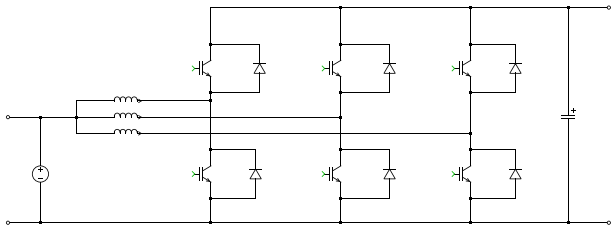

Fig. 8. Simulated model of DC/DC converter in Plecs.

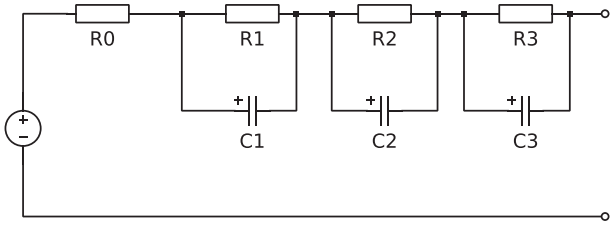

Fig. 10. Equivalent circuit with 3 R–C branches for battery cells.

Table 3
Parameters related to DC/DC converter.

parameters	values	units
switching frequency	1000	Hz
number of parallel branches	3	–
resistance of inductor pro branch	0.15	mΩ
inductance pro branch	1.3	mL
capacitor	6	mF
breakdown voltage of the semiconductor module	3300	V
rated current of the semiconductor module	450	A
thermal resistance, case to heatsink, per IGBT	17.4	K/kW
thermal resistance, junction to case, per IGBT	28.4	K/kW
thermal resistance, case to heatsink, per diode	19.3	K/kW
thermal resistance, junction to case, per diode	45.5	K/kW

fuel cell hybrid vehicles, the SoC is defined as the only one state to maintain computational load low. However, as described in Ref. [18], the handling of dynamic constraints on fuel cell systems under the one-dimensional framework makes the precondition of using dynamic programming not satisfied. Therefore, the same as [18], two-dimensional dynamic programming is used in this work. From the results of dynamic programming, the indication for developing a scalable and adaptive rule-based strategy is identified.

3.1. Basics of dynamic programming

Before using dynamic programming, the continuous model is discretized in time domain. Then the system equations can be written as follows:

$$\boldsymbol{x}[i+1] = \boldsymbol{f}(\boldsymbol{x}[i], \boldsymbol{u}[i], i), \quad i = 0, 1, 2, \ldots, T-1 \tag{4}$$

where T represents the number of time steps and i the i-th time instant, $\xi = \{\boldsymbol{u}[0], \boldsymbol{u}[1], \ldots, \boldsymbol{u}[T-1]\}$ the control series along the whole process. The total cost using this control series ξ, with $\boldsymbol{x}_0$ as the initial state value, is determined like:

$$H_{\xi}(x_0) = h(\boldsymbol{x}[T]) + \sum_{i=0}^{T-1} c(\boldsymbol{x}[i], \boldsymbol{u}[i], i)\Delta t, \tag{5}$$

where $h(\boldsymbol{x}[T])$ is the cost initialization related to the final states and the term $c(\boldsymbol{x}[i], \boldsymbol{u}[i], i)\Delta t$ represents the transition cost in the i-th time interval. The optimal control policy ξ^* is the one, that

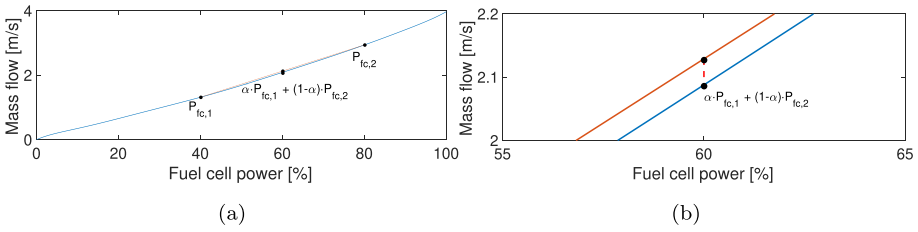

Fig. 9. Specific consumption curves of the fuel cell system: (a) Without Zoom, (b) Zoom in.

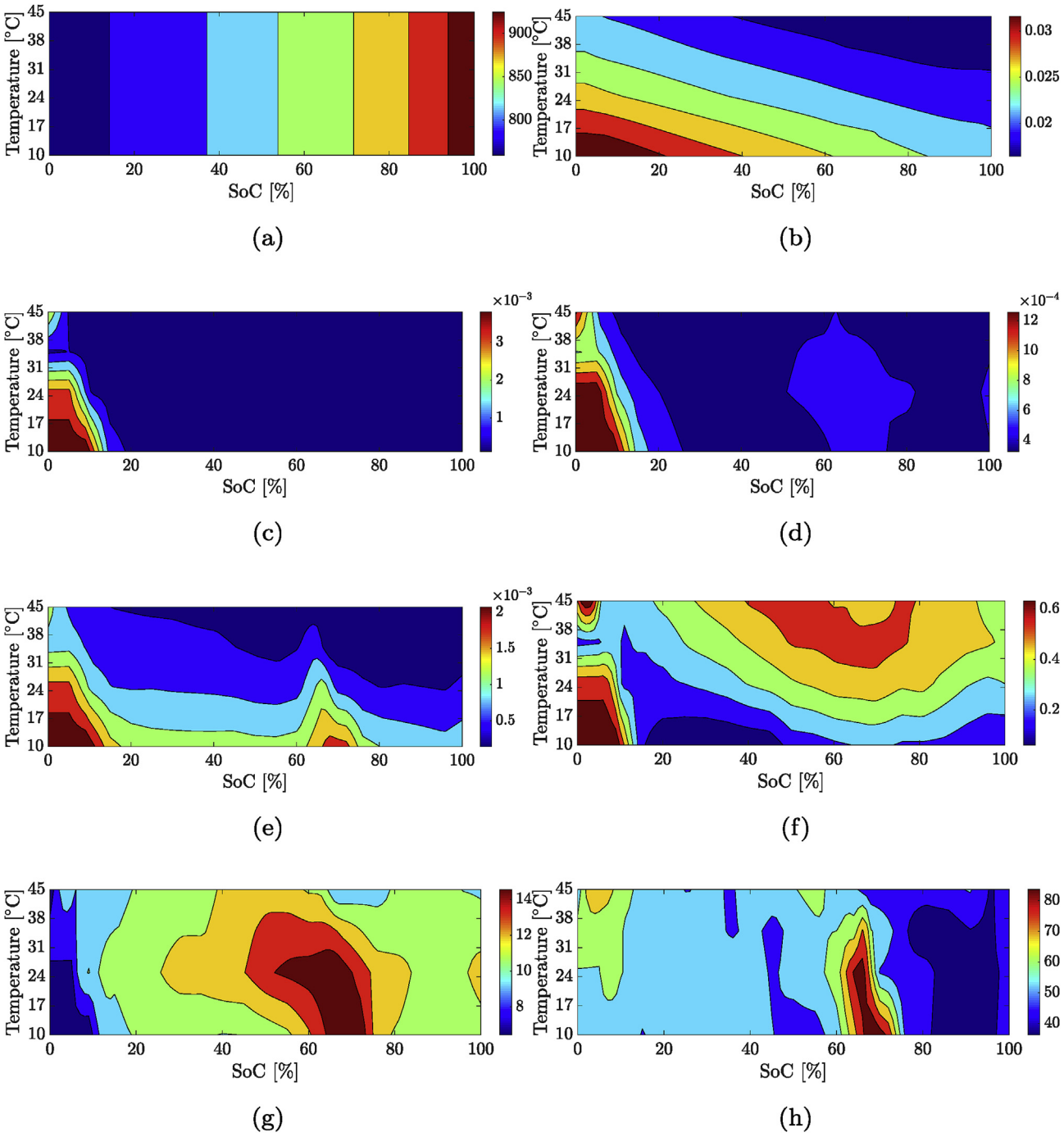

Fig. 11. Parameters of the equivalent circuit of the battery system: (a) Open-circuit voltage in V, (b) R_0 in Ω (c) R_1 in Ω, (d) R_2 in Ω, (e) R_3 in Ω, (f) Time constant due to $R_1 \cdot C_1$ in seconds, (g) Time constant due to $R_2 \cdot C_2$ in seconds, (h) Time constant due to $R_3 \cdot C_3$ in seconds.

minimizes the cost H under a provided initial state x_0 as follows:

$$H^*(x_0) = \min_{\xi \in \Xi} H_\xi(x_0), \tag{6}$$

where Ξ represents the set of all viable policies.

According to the Bellman's principle of optimality [16], the optimal cost-to-go function $H^*(\boldsymbol{x}[i])$ is determined for every node $\boldsymbol{x}[i]$ in the discretized state-time space by iterative calculations:

- Cost values at end states:

$$H^*(\boldsymbol{x}[T]) = h(\boldsymbol{x}[T]). \tag{7}$$

- Iterative calculations from $i = T-1$ until $i = 0$:

$$H^*(\boldsymbol{x}[i]) = \min_{\boldsymbol{u}[i] \in \boldsymbol{U}[i]} (c(\boldsymbol{x}[i], \boldsymbol{u}[i], i)\Delta t + H^*(\boldsymbol{x}[i+1])), \tag{8}$$

where $\boldsymbol{U}[i]$ represents the feasible control set in the i-th instant and $\boldsymbol{x}[i+1]$ is the new state, calculated by utilizing (4). After backward recursion from $i = T-1$ to $i = 0$, the optimal control series are

determined.

The exemplary implementation of dynamic programming, as found in most literature, is implemented by using embedded loops over state variables, control variables, and time steps. Its computational effort corresponds to the order of

$$\mathcal{O}\left(T \cdot j^m \cdot k^n\right), \tag{9}$$

where j and k represent the discretization degree for state and control variables, m and n the number of states and control variables respectively [30]. Therefore, the computational load is exponential proportional to the number of states and controls. Resulted from this, only the SoC is defined as the state variable in using dynamic programming to solve the offline strategies for hybrid vehicles with two energy sources, in order to maintain the computational load low, as found in most literature.

3.2. Energy management based on two-dimensional dynamic programming

In this work, as mentioned before, two-dimensional dynamic programming is implemented to consider dynamic constraints on fuel cell systems. Besides SoC, the second state variable is the fuel cell power P_{fc}. Then, the control variable is the power change rate of fuel cell systems $\frac{dP_{\mathrm{fc}}}{dt}$. It is worth mentioning that a dynamic degradation model without the three R−C branches is considered for modeling in implementing dynamic programming, to avoid introducing three more states variables of capacitor voltages, and then increase the computational load by three orders of magnitude. The energy management problem for the fuel cell hybrid trains can be formulated like:

- State vector $\boldsymbol{x} = [x_1, x_2] = [SoC, P_{\mathrm{fc}}]$,
- Control variable $u = \frac{dP_{\mathrm{fc}}}{dt}$,
- Model dynamics

$$\dot{x}_1 = -\frac{I}{Q_{\mathrm{bat}}}, \tag{10}$$

$$\dot{x}_2 = u,$$

where Q_{bat} is the battery capacity, and I the battery current, which is related to the battery power P_{bat} as follows:

$$I \cdot \left(V_{\mathrm{oc,bat}} - R_{0,\mathrm{bat}} \cdot I\right) = P_{\mathrm{bat}} = P_{\mathrm{load}} - x_2. \tag{11}$$

From that, the battery current can be written in function of the load power and the fuel cell power like:

$$I = \frac{V_{\mathrm{oc,bat}}}{2R_{0,\mathrm{bat}}} - \sqrt{\left(\frac{V_{\mathrm{oc,bat}}}{2R_{0,\mathrm{bat}}}\right)^2 - \frac{P_{\mathrm{load}} - x_2}{R_{0,\mathrm{bat}}}}. \tag{12}$$

After its substitution in (10), follow the model dynamics under the two-dimensional framework:

$$\dot{x}_1 = -\frac{1}{Q_{\mathrm{bat}}}\left(\frac{V_{\mathrm{oc,bat}}}{2R_{0,\mathrm{bat}}} - \sqrt{\left(\frac{V_{\mathrm{oc,bat}}}{2R_{0,\mathrm{bat}}}\right)^2 - \frac{P_{\mathrm{load}} - x_2}{R_{0,\mathrm{bat}}}}\right), \tag{13}$$

$$\dot{x}_2 = u,$$

Thereby, the dependency of the battery open-circuit voltage $V_{\mathrm{oc,bat}}$ and the inner resistance $R_{0,\mathrm{bat}}$ on SoC is considered.

- state constraints:

$$0.15 \le x_1 \le 0.95, \tag{14}$$

$$20\mathrm{kW} \le x_2 \le 200\mathrm{kW},$$

where the minimal power of fuel cell system is set to be 20 kW instead of zero to avoid switching off of the fue cell system and the maximal power is equal to the rated power of the fuel cell system 200 kW. It is worth mentioning that as suggested by the supplier of the fuel cell system, a minimal internal current of 10 A of the system is required to keep the system working healthily if switched on, which corresponds to the assumed minimal value of 20 kW. The limits on SoC protects the battery system from over-charging and over-discharging.

- control constraint to avoid rapid power change of fuel cell systems:

$$-5\mathrm{kW}/s \le u \le 5\mathrm{kW}/s. \tag{15}$$

It is worth mentioning that the limits can be adapted more appropriately according to the actual states of the fuel cell system. It will be shown later, that under different limits, the extraction of experience from the results of dynamic programming is not influenced. Here, they are set conservatively to realize a fully secure operation, and the effects of these limits on the fuel economy will be described later.

- battery current limits to avoid overheating and further accelerated aging of batteries

$$-900A \le I_{\mathrm{bat}} \le 900A. \tag{16}$$

The cost function with fuel economy and fuel cell aging considered is defined as follows:

$$J = \underbrace{h\left(x_1\left(t_{\mathrm{f}}\right)\right)}_{\text{initialization}} + \underbrace{\Delta t \sum_{i=0}^{T-1} \dot{m}_{\mathrm{H_2}}(x_2[i])}_{\text{fuel cell consumption}} + \underbrace{\Delta t \sum_{i=0}^{N-1} \delta |u[i]|}_{\text{change rate penalty}}, \tag{17}$$

where $h(x_1(t_{\mathrm{f}}))$ is the initialization function in terms of the final states and $\dot{m}_{\mathrm{H_2}}$ the mass flow with unit of g/s. The rapid power change of fuel cell system is penalized by factor δ in the last term. For $\delta = 0$, the cost function considers only fuel economy.

To reduce computational time, matrix-based calculation is implemented for the dynamic programming algorithm. The cost-to-go function of new states, needed in (8), is evaluated using interpolation. If the new state lies in unfeasible area, a vast number is allocated to the new state, to exclude the policy, that leads the state trajectories go through this unfeasible state point.

3.3. Results of dynamic programming and discussions

The setup parameters of two-dimensional DP are summarized in Table 4. The initial and end SoC are set to be 0.5 as the boundary conditions.

This algorithm is implemented for the three driving cycles under different weather conditions, damping factors, and the limits of fuel cell power change, and the results of power distribution and SoC trajectories are displayed.

According to the results for different driving cycles in summer, as shown in Fig. 12, it is evident that the fuel cell system maintains its power near an average one, independent on that whether the train goes uphills and downhills. Correspondingly, the power required to overcome the terrain gradient does not influence fuel cell power. In other words, the fuel cell system should work near

Table 4
Setup parameters of two-dimensional dynamic programming.

Parameters	Lower	Upper	Discretization	Number of stages
Time (s)	0	–	1	–
SoC	0.15	0.95	0.0001	8001
P_{fc} (kW)	20	200	5	37
$\frac{dP_{fc}}{dt}$ (kW/s)	−5	5	1	11

the global average load power without following the enormous power demand change due to the changeable terrain gradient. Then the battery system covers and recycles the power demand due to the gradient, and the SoC tends to increase when the train is going downhill and decrease vice versa, as shown in Fig. 12b and d.

The comparison of power distribution under different weather, including summer and winter, is shown in Fig. 13a and Fig. 13b.

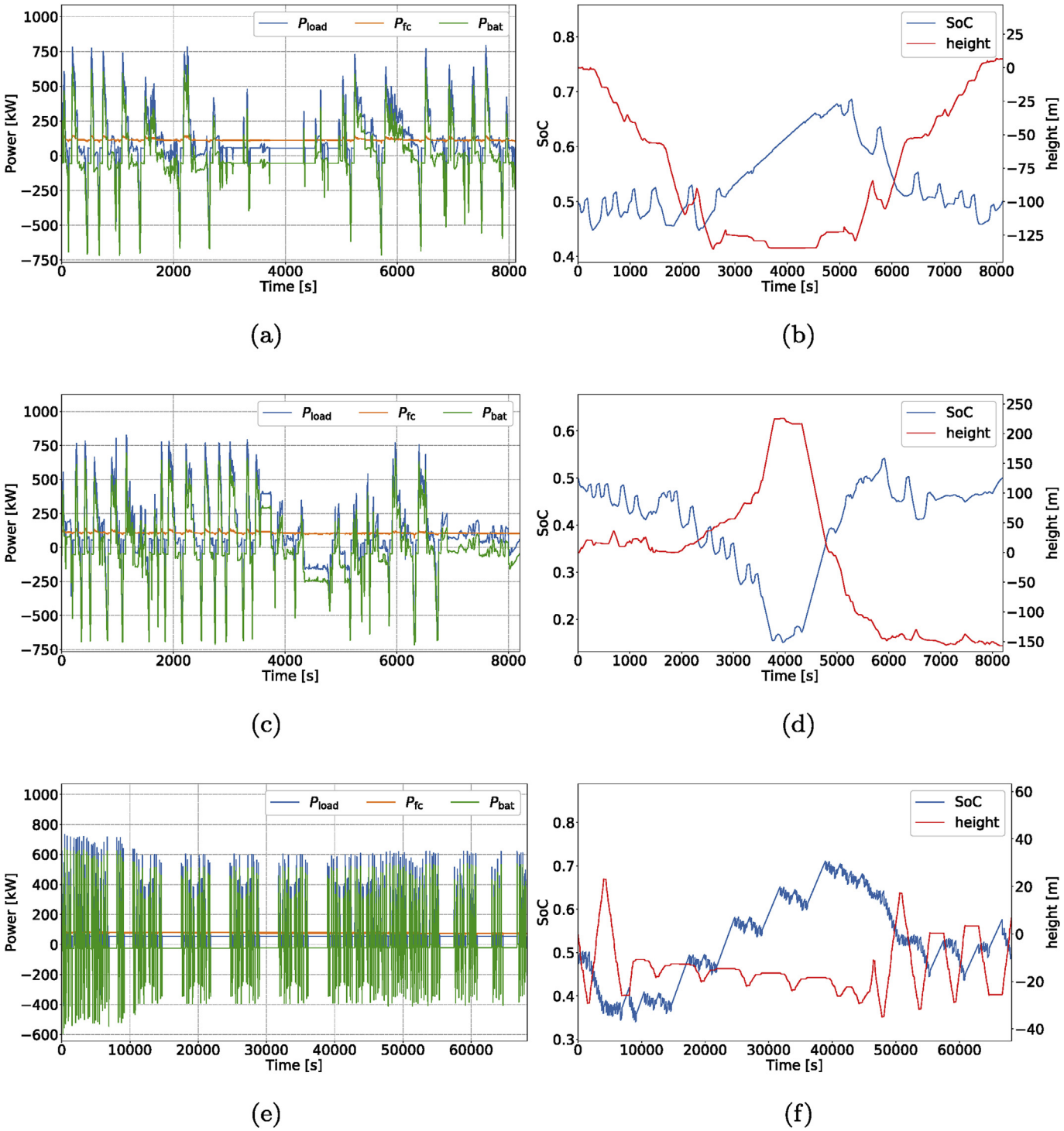

Fig. 12. Results of dynamic programming for different driving cycles in summer: (a) Power distribution for driving cycle 1, (b) SoC and height trajectories for driving cycle 1, (c) Power distribution for driving cycle 2, (d) SoC and height trajectories for driving cycle 2, (e) Power distribution for driving cycle 3, (f) SoC and height trajectories for driving cycle 3.

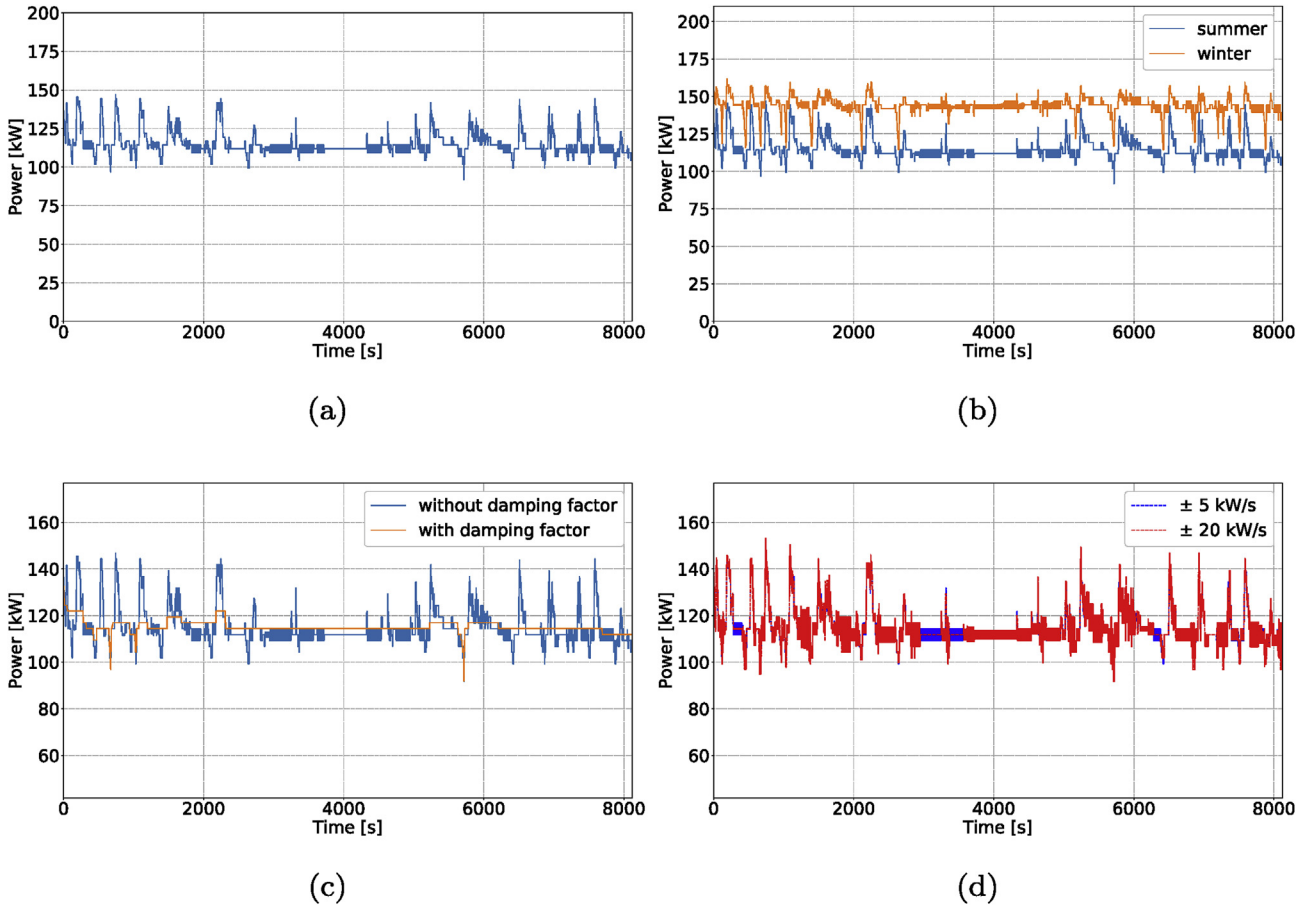

Fig. 13. Comparison regarding fuel cell power for driving cycle 1 under different weather, damping factors, and power change limits: (a) Basis of comparison, summer, $\delta = 0$, and ± 5 kW/s (b) Winter, $\delta = 0$, and ± 5 kW/s, (c) Summer, $\delta = 0.025$, and ± 5 kW/s (d) Summer, $\delta = 0$, and ± 20 kW/s.

Under both seasons, the fuel cell power is close to the average values, with the average value in winter about 30 kW higher than in summer. This increase is related to auxiliary consumption. As mentioned in modeling, the average auxiliary consumption in winter is 83 kW, compared to 55 kW in summer. The effect of the damping factor on the power distribution can be drawn from Fig. 13c. With the help of a small damping factor equal to 0.025, the fuel cell system works under a much stable operation with less dynamic. Regarding the fuel economy, the increase in total hydrogen consumption is negligible, as 16052 g under $\delta = 0.025$ compared to 16018 g under $\delta = 0$. Then it can be imagined further that the fuel cell power keeps a constant value during travel between two stations, which will be introduce into the rule-based strategy later. The effect of rate limitations on the power distribution can be drawn in Fig. 13d. The fuel cell power is almost overlapping with each other, and the hydrogen consumption difference is only 4 g. Some other results from dynamic programming are listed in Table 5. Thereby, the hydrogen consumption is scaled for the whole train instead of a half train.

Table 5
Results of dynamic programming.

Cycles	Season	δ	Limits [kW/s]	$\overline{P}_{fc}$ [kW]	H_2 [g]	H_2 [kg/km]
1	summer	0	±5	114.6	16018	0.220
2	summer	0	±5	107.9	15088	0.196
3	summer	0	±5	78.3	87905	0.301
	summer	0.025	±5	114.8	16052	0.220
1						
1	winter	0	±5	143.5	20881	0.286
1	summer	0	±20	114.6	16022	0.220

Overall, it can be drawn from the results of dynamic programming for different driving situations, that the fuel cell system should work near the global average load power, for the goodness of stable operation and fuel economy.

4. Rule-based strategies

In this section, the rule-based strategy will be derived, and its scalability, causality, and adaptivity will be emphasized.

4.1. Utilization of the convexity of specific consumption curves

The fuel cell train works without over-lines. To meet the charge-sustaining condition, the total electrical energy from the fuel cell system should be equal to the total load energy as:

$$\int_0^T P_{fc}(\tau)d\tau = \int_0^T P_{load}(\tau)d\tau, \tag{18}$$

where T is the travel time. Here, the loss in battery systems is not considered in order to simplify the to derive process. According to the power follower rules, as found in most literature about rule-based strategies, the fuel cell power varies with the load power changes. Therefore, the distribution of the working points depends on the working conditions of the hybrid train. Usually, a train

experiences mainly three different load phases: acceleration, constant speed, and regenerative braking. In the acceleration phase, the high power demand leads to a more massive fuel cell power according to the load follower rules. In the other phases, the massively reduced power demand keeps the fuel cell power low. Therefore, the working points of the fuel cell system are mainly distributed in the high and low power range, whose corresponding specific consumption is rather distributed.

In order to reduce hydrogen consumption, the convex specific consumption curve of the fuel cell system, as shown in Fig. 9, can be utilized. The inequality in (3) can be extended for the whole traveling as:

$$\dot{m}_{H_2}\left(\overline{P}_{fc}\right) < \frac{\int_0^T \dot{m}_{H_2}\left(P_{fc}(\tau)\right)\, d\tau}{T}. \tag{19}$$

Therefore, a concentration of working points near the global average load power results in less hydrogen consumption than a distribution of working points, which is consistent with the results of dynamic programming. From this, the rules of the strategy can be derived, as displayed in Fig. 14. Thereby, the fuel cell system works in mode 2 if the SoC is in medium-range, whereby the fuel cell power is maintained at the average load power. It is worth mentioning that the average value is not fixed and will be updated depending on the driving condition. If the SoC is low, the fuel cell system works in mode 1, with the fuel cell power more than the average value by factor *a*. Conversely, if the SoC is beyond an upper limit, the system works in mode 3, with the fuel cell power reduced by factor *b*. In this work, the factor *a* and *b* are 0.33 and 0.4, respectively. Furthermore, hysteresis control is implemented to avoid frequent switching between different modes, which help to reduce dynamic in the fuel cell system, as shown in Fig. 14b. Its threshold values are set with a_1, a_2, a_3, a_4 equals 0.25, 0.3, 0.85, and 0.9, respectively. These threshold values are set corresponding to the SoC limits shown in (14). Besides that, a minimum limit of 20 kW is chosen to avoid switching off of the fuel cell system during travel, and a maximum limit of 180 kW instead of the rated value is set for the derated operation of future test on test bench. It has to be mentioned that these two limits can be adjusted according to the actual state of the fuel cell system. Here, for simplicity, it is assumed to be constant with enough margin to the physical limits. These mentioned parameters can be tuned by using offline optimization. However, the strategy should be designed so that the system avoids working in mode 1 and mode 3, for the goodness of stable operation and fuel economy. This will be realized through the to be introduced mechanism of estimating the average load power. Therefore, tunning parameters is not necessary if the average load power is appropriately updated. The next task is to estimate the average load power and to integrate this average power into the strategy appropriately.

4.2. Mechanism to estimate and update average load power

The global average load power along the driving cycle is not available in real-time applications. Therefore, the history information is utilized to estimate the average load power. As before mentioned, the load power experiences massive variations in different driving phases. In the acceleration operation, the power demand is positive and significant, mainly to overcome the inertia force. In the constant speed phase, comparatively much smaller driving power is needed to cover friction forces. In the regenerative braking phase, an enormous negative load power is recycled. Therefore, In order to avoid overestimation and underestimation, the update of the average load power, used in the rules shown in Fig. 14a, takes place when the train leaves stations instead during acceleration and regenerative braking, as shown Fig. 15. In other words, the fuel cell power remains constant during traveling between two stations, which corresponds to the experience from the last section of strategies with damping factors negligible influencing fuel economy. Because the estimate of the average load power is based on the history information, as formulated in (20), the causality of the rule-based strategy is maintained. Corresponding to equation (19) this rule-based strategy realizes a high fuel economy by taking advantage of the convex characteristics of specific consumption curves. Moreover, the fuel cell system works in a much stable condition during driving between two stations, without the variant load power to follow, from that the lifetime of fuel cell systems profits.

$$\overline{P}_{load}(t) = \frac{\int_0^t P_{load}(\tau) d\tau}{t}, \tag{20}$$

4.3. Adjusting of average load power by using terrain information

The load power required to be jointly supplied by fuel cell and battery systems is

$$P_{load}(t) = F_x \cdot v + P_{loss,driveline} + P_{aux} \tag{21}$$

$$= \left(F_a + F_r + F_{air} + F_g + F_b\right) \cdot v + P_{loss,driveline} + P_{aux}.$$

With substitution of (21) into (20) follows

$$\overline{P}_{load,1}(t) = \frac{\int_0^t \left(\left(F_a + F_r + F_{air} + F_g + F_b\right) \cdot v + P_{loss,driveline} + P_{aux}\right) d\tau}{t} \tag{22}$$

where P_{aux} is the power for auxiliary devices, $P_{loss,driveline}$ the sum of power loss in the DC/DC converter, inverter, motor, gear and the rest is needed to overcome the various resistance along the driving cycle. Among them, the average amplitude of the gradient force can be more significant compared to other resistant forces except the acceleration force regarding the amplitude, as shown in Fig. 16. As mentioned in the section modeling, the driving cycle 2 has the most significant average value of the slope, while the driving cycle 3 has the least value. This enormous gradient force leads to a considerable difference in the load power between during uphills and downhills.

Therefore, the estimated average load power by using (22) is higher than the global average one, if the train first goes uphills and then go downhills, while the estimated average load power is lower than the global one reversely, which results in a bad fuel economy and oscillations of workings points of fuel cell systems.

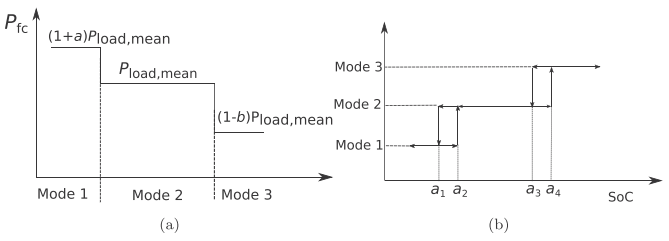

Fig. 14. Mechanism of the rule-based strategy: (a) Operation modes, (b) Hysteresis control.

As learned from the results of dynamic programming, the fuel cell system covers the average loss power during the whole travel, and the power demand due to the gradient force does not mean loss. The essential reason for that phenomenon is that the gravitational energy reserve during uphills can be recycled during downhills. Learned from this, the load power is corrected as:

$$P_{\text{load, cor}}(t) = P_{\text{load}}(t) - m \cdot g \cdot \sin\varphi(t) \cdot v(t) + m \cdot g \cdot \sin\overline{\varphi} \cdot v(t), \tag{23}$$

and the estimate of the average value can be reformulated like:

$$\overline{P}_{\text{load},2}(t) = \frac{\int_0^t \left(P_{\text{load, cor}}(\tau)\right) d\tau}{t}, \tag{24}$$

Thereby, the power to overcome the gradient force in each time instant is excluded from the determination of the average load power, and the term $m \cdot g \cdot \sin\overline{\varphi}$ represents the average gravitational force to overcome, which is related to the height difference between the start and end stations.

Another critical point is related to the long hold time of regional trains in some stations, as shown in the driving cycle 3 in Fig. 3c. The estimated average value by using (24) can lead to an enormous increase of SoC during the long hold time, which triggered the Mode 3 as defined before, because the estimation does not consider possible long hold time in future. Then, the oscillation of fuel cell systems and a worse fuel economy result. In order to solve this problem, the travel time and parking time already experienced, and the total travel time and parking time for each trip, which are available for railway transportation, are utilized to improve the estimation of the average values as follows:

$$\overline{P}_{\text{load},3}(t) = \frac{T_{\text{drive}} \cdot \underset{\text{driving}}{\int} P_{\text{load, cor}}(\tau) d\tau}{T_{\text{driven}}} + \frac{T_{\text{hold}} \cdot \underset{\text{holding}}{\int} P_{\text{load, cor}}(\tau) d\tau}{T_{\text{held}}}, \tag{25}$$

where T is the total trip time, T_{drive} the total driving time, T_{hold} the total hold time, T_{driven} the experienced driving time at each time to update the average value, T_{held} the experienced hold time, and the corrected load power is integrated to calculate the energy consumption during driving and hold separately. In this way, the estimate of the average value considers the future hold time, and the over-charging of the battery system during the long hold time can be avoided.

Furthermore, the difference between the integral of the corrected load power and the supplied fuel cell power so far should be compensated in the future estimation of the average load power, to satisfy the charge-sustaining condition, as follows:

$$\overline{P}_{\text{load},4}(t) = \overline{P}_{\text{load},3}(t) + \frac{\int_0^t \left(P_{\text{load, cor}}(\tau) - P_{\text{fc}}(\tau)\right) d\tau}{T - T_{\text{traveled}}}, \tag{26}$$

where T_{traveled} is the experienced travel time in each instant to update the average value.

Finally, the average battery loss is added to that as:

$$P_{\text{load,mean}}(t) = \overline{P}_{\text{load},4}(t) + \overline{P}_{\text{bat,loss}}(t). \tag{27}$$

This average value is implemented in mode 2 and updated each time instant when the train leaves a station in between. If the SoC end target value is different from the initial value, an average power corresponding to the difference of battery energy should be added to that, and the average value can be reformulated as:

$$P_{\text{load,mean}}(t) = \overline{P}_{\text{load},4}(t) + \overline{P}_{\text{bat,loss}}(t) + \frac{\Delta E_{\text{bat}}}{T}, \tag{28}$$

where ΔE_{bat} represents the energy difference corresponding to different SoC values of the battery system and T the total travel time.

5. Results and discussions

To evaluate this real-time available strategy, its results are compared to the results of dynamic programming with the SoC boundary values and the load power trajectory kept the same as the rule-based strategy. Because the loss in R_1, R_2, and R_3 of the battery system is not taken into account in using dynamic programming, the fuel cell power from the results of dynamic programming has to be corrected upwards by the sum of this loss. Thereby, the battery current resulted from dynamic programming is fed into the three parallel R–C branches of the battery system as shown in Fig. 17.

The corrected fuel cell power is then used to estimate mass flow and total hydrogen consumption. It is worth mentioning that the corrected fuel cell power is not entirely equivalent to optimal references. However, it can be used to evaluate the rule-based strategy without significant deviation.

In the following, the trajectories from the rule-based strategy for different driving cycles, weather, and rate limits are displayed, together with that resulted from dynamic programming. The initial

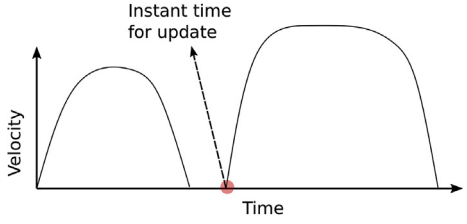

Fig. 15. Schematic explaining the time instant to update the average load power.

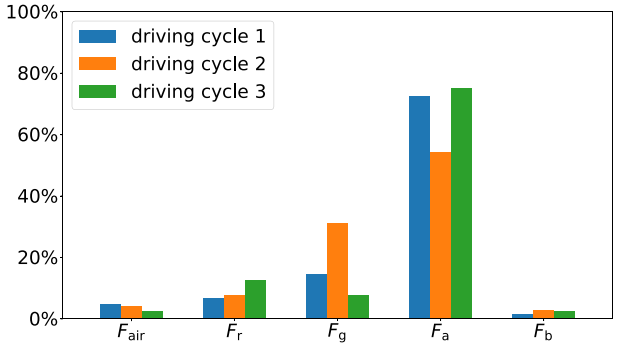

Fig. 16. Percentages of the average amplitude of different forces in total resistance force along the whole driving cycles.

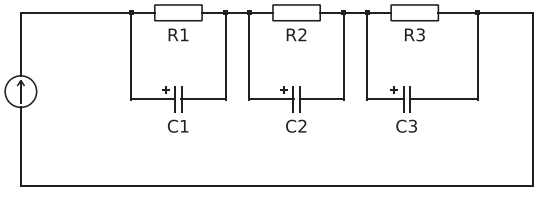

Fig. 17. Loss determination in parallel branches.

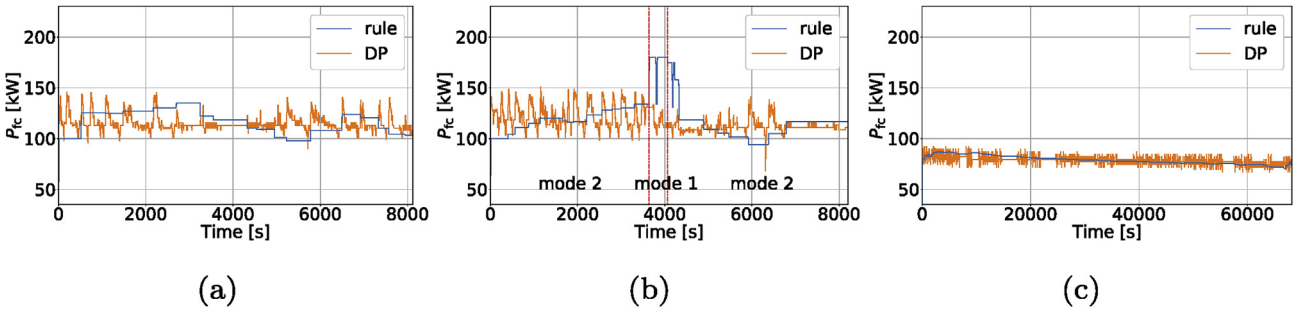

Fig. 18. Fuel cell power trajectories for different driving cycles in summer, compared to dynamic programming: (a) driving cycle 1, (b) driving cycle 2, (c) driving cycle 3.

SoC is set to be 0.5 for all simulations.

Fig. 18 displays the fuel cell power trajectories for different driving cycles in summer, compared with optimal trajectories from dynamic programming. The fuel cell system for the driving cycle 1 and 3 under the rule-based strategy works near the average values with much less oscillation than from dynamic programming. For the driving cycle 2, as the SoC meanwhile crosses the threshold values between mode 2 and mode 1, as shown in Fig. 19b, the operational mode of the fuel cell system switches from mode 2 to mode 1 with more output than the average value. Until the SoC reaches the threshold values again, the operational mode is switched back to mode 2. Regarding the fuel economy, more hydrogen consumption of 0.48%, 0.83%, and 0.01% result for the three driving cycles, respectively, as compared to the consumption by using dynamic programming. It is worth mentioning that the fuel economy under the driving cycle 2 can be improved if the fuel cell power increases in advance so that the SoC does not fall below the threshold values, and no mode switching takes place. For that purpose, the load and the terrain information in the future are required.

Fig. 19 shows comparison regarding the SoC trajectories. The SoC lies in within the accessible limits. A higher depth of discharge is observed under the rule-based strategy, compared to that under dynamic programming. The reason for that phenomenon lies in that as the fuel cell power stays near the average values under the rule-based strategy, it follows the change of load power to some degree under dynamic programming. Then, the throughput of the battery system under the rule-based strategy is more significant than under dynamic programming, which also is reflected in the depth of discharge. The small difference regarding the SoC trajectories between the rule-based strategy and dynamic programming reflects the high fuel economy of the rules.

In winter, the fuel cell power increases by about 30 kW, as the auxiliary consumption increases. The fuel cell power and SoC trajectories are compared to that from dynamic programming, as shown in Fig. 20 and Fig. 21. The fuel cell system also works near the average values with much less dynamic. Regarding the fuel economy, increase consumption of 0.38%, 0.43%, and 0.09% for different driving cycles, resulted as compared to dynamic programming. Together with the results in summer, the rule-based strategy shows the best performance regarding fuel economy for driving cycle 3 under different weather, which can be drawn especially from

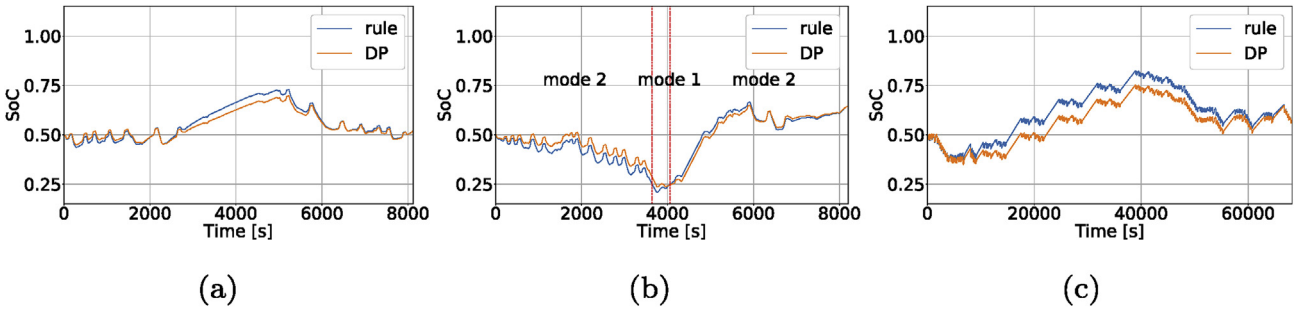

Fig. 19. SoC trajectories for different driving cycles in summer, compared to dynamic programming: (a) driving cycle 1, (b) driving cycle 2, (c) driving cycle 3.

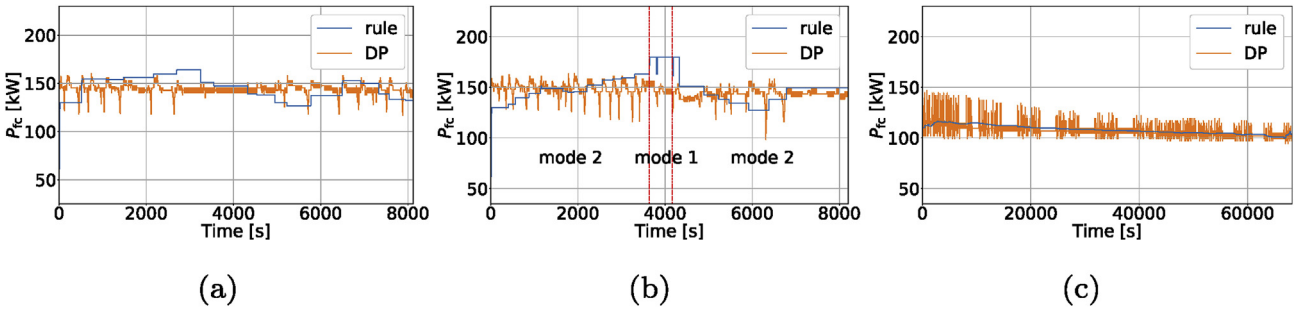

Fig. 20. Fuel cell power trajectories for different driving cycles in winter, compared to dynamic programming: (a) driving cycle 1, (b) driving cycle 2, (c) driving cycle 3.

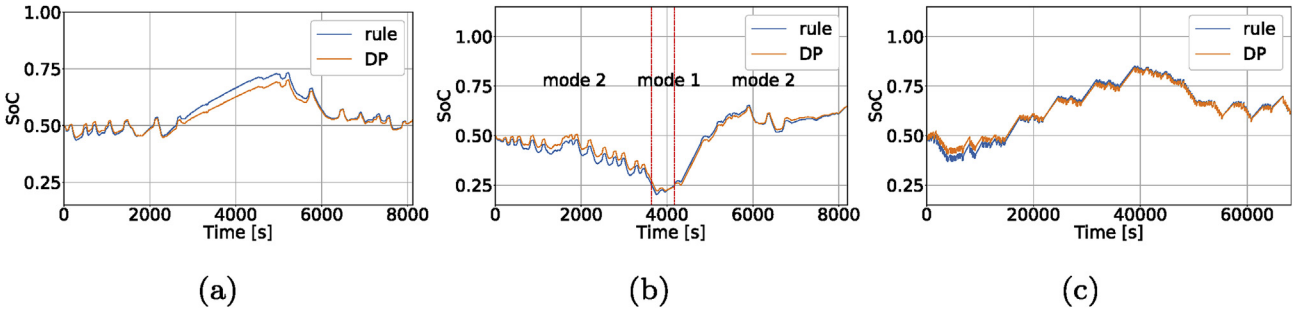

Fig. 21. SoC trajectories for different driving cycles in winter, compared to dynamic programming: (a) driving cycle 1, (b) driving cycle 2, (c) driving cycle 3.

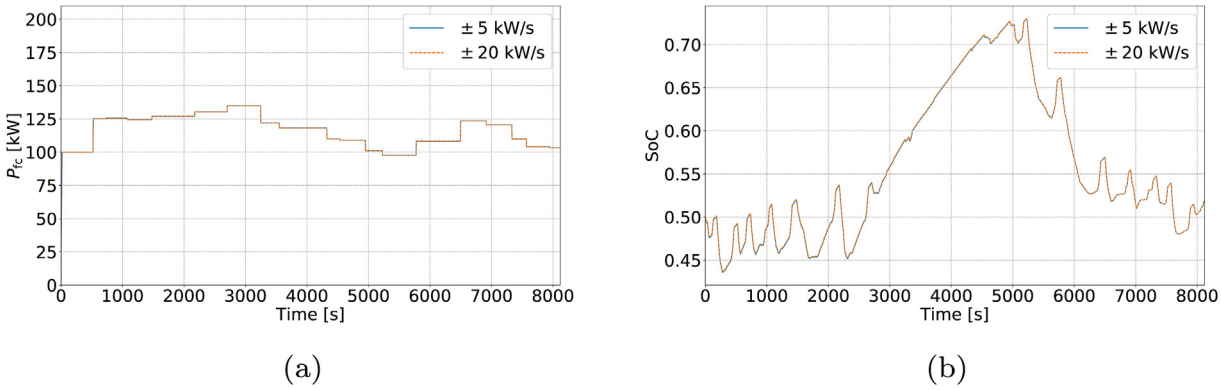

Fig. 22. Effects of rate limits of fuel cell power under driving cycle 1 in summer on: (a) Fuel cell power trajectory (b) SoC trajectory.

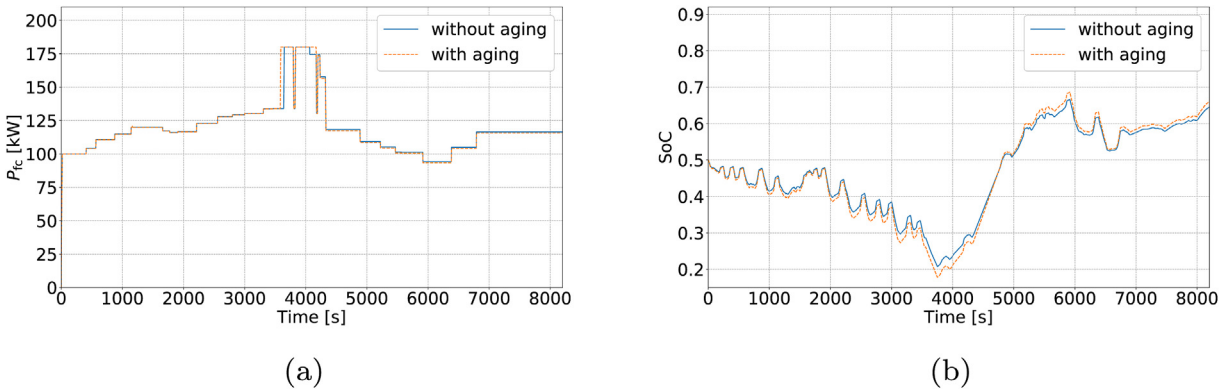

Fig. 23. Effects of battery aging under driving cycle 2 in summer on: (a) Fuel cell power trajectory (b) SoC trajectory.

Figs. 18c and 20c. Thereby, the fuel cell power trajectory is fast in the middle of the offline optimized trajectories by using dynamic programming.

In order to examine the effect of rate limits of fuel cell power on the fuel economy, the simulation with the rate limit of ± 20 kW/s is done, with its results compared to that under the limit of ± 5 kW/s, as shown in Fig. 22. The fuel cell power and SoC trajectories are almost identical, and also the fuel economy. It is evident that under the designed rules, especially with the fuel cell power controlled at a constant value between two stations, a higher rate limit brings no benefits regarding the fuel economy.

For examining the effect of component aging on the performance of the rule-based strategy, a simulation with an assumed decrease of the battery capacity of 10% is done. The results are compared to that without aging, as shown in Fig. 23. Due to the smaller capacity, the strategy is earlier switched into mode 1, and consumes more hydrogen with more dynamic than before. Consumption increase of 1.27% compared to dynamic programming is observed. To improve the performance of the strategy with components aged, the load and terrain information in the future need to be utilized, to correct the fuel cell power in advance, so that the operation of the fuel cell system out of mode 2 is avoided. This belongs to the future work.

In summary, all the results related to fuel economy and SoC are collected in Table 6, and the high fuel economy can be identified.

6. Conclusions

In this work, a scalable, causal, adaptive rule-based energy management strategy for the fuel cell hybrid train is designed, as

Table 6
Simulation results of the rule-based strategy.

Cycles	SoC_{end}	SoC_{min}	SoC_{max}	H_2 [kg/km]	Ref.DP	Notes
1, summer	0.5183	0.4358	0.7298	0.224	0.48%	–
2, summer	0.6445	0.2075	0.6657	0.221	0.83%	–
3, summer	0.5733	0.3665	0.8237	0.303	0.01%	–
1, winter	0.5236	0.4354	0.7329	0.292	0.38%	–
2, winter	0.6475	0.2035	0.6535	0.285	0.43%	–
3, winter	0.6228	0.3693	0.8504	0.431	0.09%	–
1, summer	0.5183	0.4366	0.7301	0.224	0.46%	±20
1, summer	0.5204	0.4286	0.7549	0.224	1.27%	aging

learned from the results of dynamic programming. This strategy utilizes the convexity of the specific consumption curve of fuel cell systems and maintains the fuel cell system working close to the average load power. Thereby, the average load power is estimated by using the history information, which makes the strategy causal and adaptive. Besides that, the transient power demand due to gradient slopes is excluded in the calculation to reduce oscillations of workings points of fuel cell systems along with the variable gradient. The pre-known driving time and hold time available in railway transportation are utilized to improve the estimation of the average value, to avoid overcharging of batteries during the long holding time. The functionality of this strategy, under different weather, driving, and aging conditions, is validated by comparison with the results of dynamic programming. An excellent fuel economy under a typical driving cycle of regional railway vehicles in Berlin, with only 0.01% and 0.09% more consumption in summer and winter respectively, compared to the results of dynamic programming, is resulted. Moreover, the fuel cell system works with much fewer oscillations, from which the lifetime of the fuel cell system benefits. Due to the components-based characteristics, the strategy can be scaled or transferred to other configuration systems or driving conditions without loss of effectiveness. In the future, the average load power can be more appropriately estimated by using terrain and load information about upcoming routes.

CRediT authorship contribution statement

Hujun Peng: Conceptualization, Methodology, Formal analysis, Writing - original draft. **Jianxiang Li:** Software, Data curation. **Andreas Thul:** Project administration, Writing - review & editing. **Kai Deng:** Writing - review & editing. **Cem Ünlübayir:** Writing - review & editing. **Lars Löwenstein:** Writing - review & editing. **Kay Hameyer:** Supervision, Writing - review & editing.

References

[1] Railway electrification: Germany only average, https://www.allianz-pro-schiene.de/en/press-releases/2012-19-electric-transport-federal-government-still-has-homework-/_to-do/, accessed December 18, 2019.
[2] Jr east to trial fuel cell multiple-unit. https://www.railwaygazette.com/news/news/asia/single-view/view/jr-east-to-trial-toyota-powered-fuel-cell-multiple-unit.html. [Accessed 18 December 2019].
[3] Jürgen H. Auf dem weg zur null-emmision, eisenbahn-magazin. 2017. p. 41. 7.
[4] Brennstoffzellen. Siemens beauftragt ballard power. https://www.iwr.de/news.php?id=34729. [Accessed 18 December 2019].
[5] Fletcher T, Thring R, Watkinson M. An energy management strategy to concurrently optimise fuel consumption & pem fuel cell lifetime in a hybrid vehicle. Int J Hydrogen Energy 2016;41(46):21503–15.
[6] Sulaiman N, Hannan MA, Mohamed A, Ker PJ, Majlan EH, Wan Daud WR. Optimization of energy management system for fuel-cell hybrid electric vehicles: issues and recommendations. Appl Energy 2018;228:2061–79.
[7] Tran D-D, Vafaeipour M, El Baghdadi M, Barrero R, van Mierlo J, Hegazy O. Thorough state-of-the-art analysis of electric and hybrid vehicle powertrains: topologies and integrated energy management strategies. Renew Sustain Energy Rev 2019:109596.
[8] Zhang P, Yan F, Du C. A comprehensive analysis of energy management strategies for hybrid electric vehicles based on bibliometrics. Renew Sustain Energy Rev 2015;48:88–104.
[9] I. Pielecha, W. Cieślik, A. Szałek, The use of electric drive in urban driving conditions using a hydrogen powered vehicle-toyota mirai, Combustion Engines 57.
[10] Wang Y, Sun Z, Chen Z. Development of energy management system based on a rule-based power distribution strategy for hybrid power sources. Energy 2019;175:1055–66.
[11] Wang Y, Li X, Wang L, Sun Z. Multiple-grained velocity prediction and energy management strategy for hybrid propulsion systems. Journal of Energy Storage 2019;26:100950.
[12] Wang Y, Sun Z, Chen Z. Energy management strategy for battery/supercapacitor/fuel cell hybrid source vehicles based on finite state machine. Appl Energy 2019;254:113707.
[13] Wang Y, Sun Z, Li X, Yang X, Chen Z. A comparative study of power allocation strategies used in fuel cell and ultracapacitor hybrid systems. Energy 2019;189:116142.
[14] Caux S, Hankache W, Fadel M, Hissel D. On-line fuzzy energy management for hybrid fuel cell systems. Int J Hydrogen Energy 2010;35(5):2134–43.
[15] Song Z, Hofmann H, Li J, Han X, Ouyang M. Optimization for a hybrid energy storage system in electric vehicles using dynamic programing approach. Appl Energy 2015;139:151–62.
[16] Bellman R. The theory of dynamic programming. Bull Am Math Soc 1954;60(6):503–15.
[17] Ansarey M, Panahi MS, Ziarati H, Mahjoob M. Optimal energy management in a dual-storage fuel-cell hybrid vehicle using multi-dimensional dynamic programming. J Power Sources 2014;250:359–71.
[18] Peng H, Li J, Deng K, Thul A, Li W, Löwenstein L, Sauer DU, Hameyer K. An efficient optimum energy management strategy using parallel dynamic programming for a hybrid train powered by fuel-cells and batteries. In: 2019 IEEE vehicle power and propulsion conference (VPPC); 2019. p. 1–7.
[19] Paganelli G, Delprat S, Guerra T-M, Rimaux J, Santin J-J. Equivalent consumption minimization strategy for parallel hybrid powertrains. In: Vehicular technology conference. IEEE 55th vehicular technology conference. VTC spring 2002 (cat. No. 02CH37367), vol. 4. IEEE; 2002. p. 2076–81.
[20] Pei D, Leamy MJ. Dynamic programming-informed equivalent cost minimization control strategies for hybrid-electric vehicles. J Dyn Syst Meas Contr 2013;135(5):051013.
[21] Tian X, Cai Y, Sun X, Zhu Z, Xu Y. An adaptive ecms with driving style recognition for energy optimization of parallel hybrid electric buses. Energy 2019;189:116151.
[22] Rezaei A, Burl JB, Solouk A, Zhou B, Rezaei M, Shahbakhti M. Catch energy saving opportunity (ceso), an instantaneous optimal energy management strategy for series hybrid electric vehicles. Appl Energy 2017;208:655–65.
[23] Onori S, Tribioli L. Adaptive pontryagin's minimum principle supervisory controller design for the plug-in hybrid gm chevrolet volt. Appl Energy 2015;147:224–34.
[24] Xie S, Hu X, Xin Z, Brighton J. Pontryagin's minimum principle based model predictive control of energy management for a plug-in hybrid electric bus. Appl Energy 2019;236:893–905.
[25] Ali AM, Söffker D. Towards optimal power management of hybrid electric vehicles in real-time: a review on methods, challenges, and state-of-the-art solutions. Energies 2018;11(3):476.
[26] Coradia ilint: alstoms emissionsfreier zug. http://www.igkandertalbahn.de/pdf/Main-Doku-Coradia%20iLint%20Alstom_dt-UG_StS_TK.pdf. [Accessed 18 December 2019].
[27] Hu X, Murgovski N, Johannesson L, Egardt B. Energy efficiency analysis of a series plug-in hybrid electric bus with different energy management strategies and battery sizes. Appl Energy 2013;111:1001–9.
[28] Serrao L, Onori S, Rizzoni G. A comparative analysis of energy management strategies for hybrid electric vehicles. Proc Inst Mech Eng - Part D J Automob Eng 2011;133(3):60.
[29] Liu W, Deng Q, Huang W, Liu R. Variation in cooling load of a moving air-conditioned train compartment under the effects of ambient conditions and body thermal storage. Appl Therm Eng 2011;31(6–7):1150–62.
[30] Kirk D. Optimal control theory: an introduction. Dover Books on Electrical Engineering Series, Dover Publications; 2004.